On the feasibility of monitoring carbon monoxide in the lower troposphere from a constellation of Northern Hemisphere geostationary satellites: global scale assimilation experiments (Part II)

Jérôme Barré[1], David Edwards[1], Helen Worden[1], Avelino Arellano[2], Benjamin Gaubert[1], Arlindo Da Silva[3], William Lahoz[4], Jeffrey Anderson[1]

[1] National Center for Atmospheric Research (NCAR), Boulder, CO, USA
[2] University of Arizona, Tucson AZ, USA
[3] NASA Goddard Space Flight Center, Greenbelt, MD, USA
[4] NILU, Kjeller, Norway

Corresponding Author:
Jérôme Barré, Phone: 303-497-1866, Fax: 303-497-1400
barre@ucar.edu

Abstract

This paper describes the second phase of an Observing System Simulation Experiment (OSSE) that utilizes the synthetic measurements from a constellation of satellites measuring atmospheric composition from geostationary (GEO) Earth orbit presented in part I of the study. Our OSSE is focused on carbon monoxide observations over North America, East Asia and Europe where most of the anthropogenic sources are located. Here we assess the impact of a potential GEO constellation on constraining northern hemisphere (NH) carbon monoxide (CO) using data assimilation. We show how cloud cover affects the GEO constellation data density with the largest cloud cover (i.e., lowest data density) occurring during Asian summer. We compare the modeled state of the atmosphere (Control Run), before CO data assimilation, with the known "true" state of the atmosphere (Nature Run) and show that our setup provides realistic atmospheric CO fields and emission budgets. Overall, the Control Run underestimates CO concentrations in the northern hemisphere, especially in areas close to CO sources. Assimilation experiments show that constraining CO close to the main anthropogenic sources significantly reduces errors in NH CO compared to the Control Run. We assess the changes in error reduction when only single satellite instruments are available as compared to the full constellation. We find large differences in how measurements for each continental scale observation system affect the hemispherical improvement in long-range transport patterns, especially due to seasonal cloud cover. A GEO constellation will provide the most efficient constraint on NH CO during winter when CO lifetime is longer and increments from data assimilation associated with source regions are advected further around the globe.

1. Introduction

Observing system simulation experiments (OSSEs) are a powerful method for evaluating the impact of potential future observations (Edwards et al., 2009; Timmermans et al., 2015). In Barré et al., 2015a (hereafter, Part I), we introduced the OSSE framework and method to simulate observations for a future constellation of geostationary (GEO) satellites. The OSSE results presented in this second part of the study focus on assimilation of the simulated carbon monoxide (CO) observations and evaluation of the impact on chemical weather prediction in the northern hemisphere (NH) troposphere. Because CO is a primary pollutant, with significant sources from industrial and urban fossil/biofuel burning, wildfires and biomass burning, it is a convenient chemical tracer for assessing the utility of assimilated GEO measurements for quantifying pollution emissions and their subsequent transport.

We observe high CO concentrations in the lower troposphere and in the NH due to urban and industrial pollution, over East China, India, Western Europe and the United States. Other major sources of CO in the NH are wildfires that occur during dry seasons; e.g., May to October in extratropical northern latitudes, especially in forested boreal regions. CO is also a reactive chemical compound with chemical production and destruction mainly due to hydrocarbon and hydroxyl radical (OH) oxidation, respectively. OH availability governs CO lifetime, which is shorter during summer and over low latitudes, and longer during winter and over high latitudes in the NH (Edwards et al., 2004). Satellite instruments can observe CO plumes from strong emission sources on global scales, travelling distances that depend on CO lifetime (weeks to months). This makes CO an excellent candidate for tracking fossil fuel and biomass burning emissions as they are transported from the sources into the global troposphere. The OH seasonal cycle leads to a CO build-up at the end of the NH winter, commonly underestimated in model simulations (e.g., Stein et al. 2014). This bias is likely due to a combination of factors, including an underestimation of the magnitude of the emissions, biases in the OH fields, as well as transport errors (e.g., Jiang et al., 2013; Strode et al. 2015). Data assimilation of CO, i.e. representing the best CO estimate of the atmosphere using models and observations, has many applications ranging from air quality characterization, emissions estimation, large-scale pollutant transport, and climate evolution due to changing atmospheric composition.

Part I of this study demonstrated the feasibility of simulating CO observations from three instruments with characteristics similar to the Measurement of Pollution in The Troposphere (MOPITT) instrument flying on the NASA Terra satellite. These three CO instruments would cover the most populated and hence most polluted areas of the world: Continental US (CONUS), Western Europe and Eastern Asia. Measurement simulations provide realistic multispectral sensitivities peaking at the surface during daytime for land observations. These simulated measurements also provide errors and cloud coverage at variable horizontal resolution for assimilation experiments. Previous OSSE studies assessed the impact of GEO instrument capabilities using data assimilation, but with a focus on the regional scale. Edwards et al., 2009 and Zoogman et al., 2011, 2014a,b focused on CONUS CO and ozone (O_3), while Claeyman et al., 2011 assimilated GEO measurements of CO and O_3 over Europe and Yumimoto, 2013 assimilated GEO measurements of CO over East Asia.

In part II of this study, we assimilate simulated observations from a GEO constellation composed of the three instruments defined in Part I into a global chemistry model to assess the global-scale impacts of GEO satellites for the first time. The focus of this paper is to quantify the potential of a GEO constellation for constraining NH CO distributions, especially in the lower troposphere near anthropogenic sources. We present results from two data assimilation experiments during summer and winter. Observations from each GEO instrument are assimilated independently and jointly to evaluate the impact of observations in each domain as compared to the full constellation

Section 2 of this paper further describes the OSSE framework introduced in Part I, with details on the nature run and the control run. We briefly summarize the observation simulations covered in detail in Part I, focusing here on cloud cover variability over different regions and different seasons. We also present the data assimilation methodology following Barré et al., 2015b. Section 3 gives a detailed evaluation of the GEO constellation performance due to each instrument with assimilation results such as increments, global impact on CO errors and skill score metrics. Section 4 concludes with seasonal and geographical observational requirements for a GEO constellation of CO measurements and perspectives on future work using our OSSE framework.

2. OSSE Setup

An OSSE comprises several elements (see part I, figure 1): a Nature Run (NR) that represents the atmospheric true state; an observation simulator that samples the NR to produce synthetic observations; a Control Run (CR) that is the modeled state of the atmosphere; and an assimilation system that merges the synthetic observations with the CR to produce an Assimilation Run (AR). By comparing the NR, CR and AR one can assess the impact of a new instrument concept, in this case a constellation of GEO satellites over the NH.

2.1 Nature run and control run description

The GEOS5 Nature Run (NR) used for simulating the GEO constellation observations is described in Part I of this paper and complete details and validation documents are available at http://gmao.gsfc.nasa.gov/projects/G5NR/. In this section, we focus on how we model and parameterize the NR CO concentrations and emissions. For this study, we use reduced horizontal resolution (0.5° × 0.5°) derived from the high horizontal resolution run (0.06˚ × 0.06˚) that simulates year 2006 atmospheric conditions. The NR uses a simplified version of CO chemistry as described in Ott et al., 2010. The only sink for CO is the reaction with OH. Tropospheric OH is parameterized using OH monthly means from previous calculations (also for year 2006) of a full chemical mechanism (Duncan et al., 2000). It was necessary to increase the CO emissions from fossil fuels, biofuels and biomass burning by 20%, 19% and 11%, respectively, to account for CO production from non-methane hydrocarbons emitted from these sources. We use monthly mean methane fields to calculate CO produced by methane oxidation as described in Bian et al., 2007.

Detailed descriptions of emissions are provided in Putman et al., 2014. Biogenic and methane sources of CO are taken from a coarse resolution (4° x 5°) chemical transport model simulations, while biomass burning and fossil fuel emissions were produced at 0.1° to introduce spatial heterogeneity into the simulations. We obtain daily CO biomass burning emissions from the Quick Fire Emissions Dataset (QFED) version 2.4-r6 and CO anthropogenic emissions are mainly from the Emissions Database for Global Atmospheric Research (EDGAR). We have disaggregated these emissions in time (yearly to monthly time scales) using information on the seasonal cycle of fossil fuel emissions from Bey et al., 2001. We apply no diurnal or weekly variation to the EDGAR emission inventory.

We evaluate NR mixing ratios using a combination of surface and satellite observations. In general, the NR tends to underestimate CO mixing ratios, especially during extratropical NH spring. We improve significantly these underestimates through application of an empirically derived bias correction method as described in http://gmao.gsfc.nasa.gov/projects/G5NR/TM2014-104606v36.pdf, leading to a reduced overall bias of 10% at NH extratropical latitudes compared to MOPITT CO observations. The NR succeeds in capturing major CO features due to fossil fuel emissions and biomass burning that are seen in the observations.

We use the Community Atmospheric Model with Chemistry (CAM-chem) version 5 with on-line meteorology (using CAM5 physics, Conley et al. (2012)) and on-line full gas phase chemical mechanism (MOZART-4 tropospheric chemistry) as the Control Run (CR) and as a basis for the Assimilation Runs (AR). In this study, we use a horizontal resolution of (1.25° longitude by 0.9° latitude) with 30 vertical levels from the surface up to 4hPa. Emmons et al. 2010, describes and evaluates the MOZART-4 chemical scheme; Lamarque et al. (2012) and Tilmes et al. (2015) describe updates to this scheme. The tropospheric version of the MOZART mechanism includes 85 gas-phase species, 12 bulk aerosol compounds, 39 photolysis and 157 gas-phase reactions. We prescribe the relevant chemical variables in the stratosphere, between 50 hPa and the top of the model, using climatology. Lamarque et al. (2012), Tilmes et al. (2015) and Barré et al. (2015b) showed that the modeled CO distribution at high NH latitudes is underestimated by values ranging from 25% to 75% when compared to surface, aircraft and satellite observations, indicating an underestimation of CO emissions and possibly also an overestimate of the CO loss by OH. Barré et al. (2015b) showed that assimilation of infrared Low Earth Orbiter (LEO) sounder observations partially or totally corrects the CR CO bias depending on sounder spatial coverage and vertical sensitivity.

We base the CAM-Chem anthropogenic emissions on the Atmospheric Chemistry and Climate Model Intercomparison Project (ACCMIP) historical emissions (1960-2000) and RCP 8.5 future scenario emissions (Lamarque et al., 2010). We use biomass-burning emissions provided by the Fire Inventory from NCAR version 1.5 (FINNv1.5; Wiedinmyer et al., 2011). We generate biogenic emissions offline using the global Model of Emissions of Gases and Aerosols from Nature (MEGAN v2.1; Guenther et al., 2012) and use monthly averages of daily emissions from MEGAN and FINN emitted at the surface level. Using a monthly average for the fire emission inventory is a likely source of error given that fires have daily evolving signatures. However, monthly emissions are justified in a global scale approach with coarse horizontal resolution where large-scale fire signatures last several months.

Figure 1. shows the seasonal tropospheric CO averages from the NR and CR for the winter and summer cases. Compared to the NR, the CR underestimates the CO field by 20% to 30% at extratropical NH latitudes. Underestimates of this magnitude are common in CO simulations as demonstrated by Shindell et al. (2006) who compared CO fields generated by 26 chemical transport models. As stated above, CO is primarily emitted in the troposphere from anthropogenic and biomass burning emissions. However, a significant fraction of tropospheric CO is produced from chemical oxidation and removed through its reaction with OH. Figure 1. also shows the correlation coefficients between the NR and CR for the two seasons of interest. Correlation coefficients range from 0.3 to 0.8 depending on the season and regions in the northern hemisphere. These values are also in the range of what has been previously shown by Shindell et al. (2006), Table 4, which gives correlations ranging from 0.3 to 0.9 for comparisons of chemical transport models with MOPITT CO data. Overall, we find the CR errors to be realistic in terms of bias and variability.

Figure 2. shows emission budgets over the three regions of interest (fields of regard of the 3 GEO instruments, see Part I figure 4): North America, Western Europe and Eastern Asia. We display the total emissions (anthropogenic + biomass-burning + biogenic) and the biomass-burning fraction. The differences between NR and CR emissions budgets are representative of current model capabilities since fossil fuel emissions inventories are mostly underestimated (Shindell et al., 2006). Limitations in state-of-the-art models lead to large uncertainties when characterizing biomass-burning emissions from fire events (Wiedinmyer et al., 2011) and hence large differences between the CR and NR. In most cases, there is an underestimation of CR emissions compared to the NR (for both total emissions and biomass burning emissions), except for Eastern Asia where very intense fires take place over Northern Thailand, Myanmar and Laos in NH spring. For South East Asian fires, the CR largely overestimates the fire emissions compared to the NR. This is reflected in the emission budgets in Figure 2., i.e., the March budget over Asia. In our OSSE framework, this fire occurrence over Asia provides a case study that allows assessment of how well GEO satellite data assimilation constrains the atmospheric CO state under a change of sign in the emission bias.

In summary, differences between the NR and CR are within the range of differences between state-of-the-art models and observations.

2.2 Simulated CO observations

Part I of this study provided a full description of the synthetic observations simulated from the NR and showed the instrument footprints, sensitivity and errors, and impacts of cloud cover on pixel resolution. Part I focused on July 2006 and described the three instruments are that are envisioned: GEO-US (North America), GEO-EU (Western Europe) and GEO-AS (Eastern Asia). The reader should refer to Part I for more details about the observation simulations. In this Part II paper, we extend the observation simulation data set to January, February, March (JFM) and June, July, August (JJA) 2006.

Cloud cover is important as it limits the capability of a remote sensing instrument to monitor tropospheric composition. Figure 3 displays the three instrument footprints and the cloud free ratio for JFM and JJA, 2006. The cloud free ratio is the number of cloud free occurrences over the total number of possible measurements for a given pixel. Over the three observational domains, differences of cloud free ratio between winter and summer are large. Europe and North America show more data coverage during summer than winter. This tendency is reversed for Asia. Over extratropical latitudes, summer is generally significantly less cloudy than winter due to warmer air that can retain more water vapor. Over Asia, the GEO instrument field of view (see part I figure 4) tends to cover tropical and subtropical regions, and is subject to the Asian monsoon during summer, which is a relatively wet season. For GEO-AS, winter is drier than summer with fewer clouds and more data coverage.

The geographical structure of data coverage changes with season and exhibits complex patterns. GEO-EU shows a North-South coverage difference with high coverage at southern latitudes and almost no observations northward of 50°N during the winter. Good coverage over the Mediterranean is even higher during summer. GEO-US shows very low winter coverage over New England and the Great Lakes area but reasonable coverage (above 30%) elsewhere. Summer provides overall good coverage (above 30%) and excellent coverage (above 80%) over California. GEO-AS shows patterns that are more complex, e.g., very high coverage and very low coverage over the southwest part of the domain and over the Japanese east coast, a North-South coverage difference that is less marked over winter than in summer. Overall, land data coverage is higher in winter than in summer over Asia.

2.3 Assimilation system and global OSSE design

2.3.1 Synthetic meteorological observations

In this OSSE framework we use the Data Assimilation Research Testbed (DART, Anderson et al. 2009), which is a community data assimilation software package developed since 2002 at the National Center for Atmospheric Research (NCAR). DART implements the Ensemble Kalman Filter (EnKF) technique originally introduced by Evensen (1994). This software is designed to provide high modularity that allows an easy interface for a variety of models. It facilitates ensemble-based data assimilation (DA) without needing to construct a model adjoint and adjoints for observation operators as in the case of 4D variational-based DA.

DART assimilates meteorological and chemical observations simultaneously. The data assimilation setup is based on the work of Raeder et al. (2012) for the meteorology assimilation and Barré et al. (2015b) (see supplementary information document) for the chemistry-meteorology assimilation, where conventional NOAA/NCEP meteorological observations are assimilated. These two studies provide a detailed evaluation of the performance of the meteorological analysis produced with the DART setup. In this present study, we generate synthetic conventional meteorological observations by sampling the nature run variables (winds, temperature and specific humidity) at real observation locations. We define the error characterization of synthetic observations using the ratio of the real observation error over the measurement value. We then add random noise to the sampled nature run values according to the specified error of the synthetic observations. We use the following relationships to generate synthetic meteorological observations:

$$X_s = X_t + \varepsilon \qquad (1)$$

$$\varepsilon = \mathcal{N}(0,1).\ e_s \qquad (2)$$

$$e_s = X_t\ .\ e_m\ .\ X_m^{-1} \qquad (3)$$

Where X_s is the synthetic observation value, X_t the nature run sampled at the real observation location, ε the measurement noise, e_s the synthetic observation error, e_m the real observation error and X_m the real observation value and $\mathcal{N}(0,1)$ a standard normal distribution. For meridional (V) and zonal (U) wind simulated measurements, we take into account the wind speed ($\sqrt{U^2 + V^2}$), to avoid infinite or very large ratios when calculating the ratio $X_t\ /X_m$ in equation 3. In the OSSE experiments, the CR assimilates only meteorological data, while the ARs assimilate both meteorological and CO data. The following section describes the experimental design of this study.

2.3.2 GEO constellation CO assimilation experimental design

Barré et al. (2015b) provides a complete description of the chemical data assimilation setup with a focus on CO and shows the results and evaluation with independent measurements from assimilating the MOPITT and the Infrared Atmospheric Sounding Interferometer (IASI) instrument retrieved CO profiles into the CAM-Chem model. That paper highlights the different capabilities of the IASI and MOPITT instruments with particular attention to instrument vertical sensitivity and coverage and their impact on the analysis of global CO atmospheric composition. Barré et al. (2015b) showed that satellite observations that have frequent revisit and enhanced vertical sensitivity toward the surface close to sources provide an efficient constraint and generate a global improvement in tropospheric CO concentrations. In the present study, we use the same MOPITT CO data assimilation setup to assimilate a geostationary constellation of simulated MOPITT-like measurements. Although it is possible to infer changes in the concentrations of other chemical species, here we only adjust CO concentrations using data assimilation of CO observations, as in Barré et al. (2015b).

We assimilate the full GEO constellation and each instrument independently in order to assess the global impact of the constellation and understand the contribution of each instrument to the estimation of the NH CO field. These assimilation experiments are repeated over the winter and summer 2006 (January-February-March and June-July-August, respectively) because emissions, cloud cover and CO chemical lifetime change significantly throughout the year. We hereafter name the different assimilation runs as follows:

- Control run (CR): we assimilate only meteorological data;

- Full constellation assimilation run (AR0): we assimilate meteorological and 3 GEO instrument data;
- GEO-US assimilation run (AR1): we assimilate meteorological and US GEO instrument data;
- GEO-EU assimilation run (AR2): we assimilate meteorological and European GEO instrument data;
- GEO-AS assimilation run (AR3): we assimilate meteorological and Asian GEO instrument data.

3. Results

3.1 Data assimilation increments

In this section, we investigate the overall constraint on model CO fields from the AR0 assimilation experiment during winter and summer. Figure 4 displays the root-mean-square (RMS) of the relative increments (posterior minus prior normalized by the prior) over a month for the 6-hourly data assimilation window. As described in Barré et al. (2015b) CO retrievals are assimilated every 6 hours and the RMS of the relative increments over a month is useful for identifying the overall magnitude of the CO changes due to assimilation, and for detecting short-term systematic error patterns in the CR. Please refer to Barré et al. (2015b) for additional details about the data assimilation setup.

We can observe seasonal differences in the magnitude of the increments. Three main factors can explain this difference: cloud coverage, CO model error and hence CO emissions error, and instrument sensitivity. During winter over Europe and North America, relative increments are smaller than during summer because we assimilate less data due to higher cloud cover. Conversely, Asia has the opposite tendency with relative increments that are larger over winter due to less cloud cover (see section 2.2 and Figure 3). In general, errors in CO emissions tend to be larger during the summer than during the winter (Figure 2). This also explains larger increments during the summer. Confirmation of this comes from relative increments showing structural patterns related to emission patterns. For example, we observe large relative increments over the Northeast United States (New England and slightly lower latitudes) where there are large anthropogenic CO emissions throughout the year due to high urbanization in this area. We also observe large relative increment patterns around the Bohai Sea (near Beijing) where urbanization is very high as well.

We also capture fire structures in the data assimilation relative increments; these are visible over South East Asia during winter where we detect very strong fire occurrences. Emission budgets in Figure 2 show that the CR overestimates this fire source compared to the NR. We detect other fire patterns over North America and Europe during summer, e.g., Central North US, North West US and Spain. We can also explain relative increment magnitudes in Figure 2 from differences between the CR and NR emission budgets. If the differences in the emission budget are large in a given region, then the magnitude of the data assimilation relative increments is also likely to be large.

We note that instrument sensitivity is the least dominant factor in relative increment size. We calculated the seasonal average degrees of freedom for signal (DFS), which represents the independent vertical information in the measurement throughout the troposphere, (see part I for details). GEO-US shows a DFS of 1.53 (1.28) during the winter (summer), GEO-EU shows a DFS of 1.40 (1.30) during the winter (summer) and GEO-AS shows a DFS of 1.61 (1.36) during the winter (summer). DFS depends primarily on thermal contrast and CO abundance and for these observational domains, there is clearly weaker instrument sensitivity during the summer. However, the seasonal differences in sensitivity are not so large that they dominate the relative size of increments found for summer versus winter.

Diagnosing data assimilation relative increments shows that a GEO constellation provides an efficient constraint on atmospheric CO on continental scales at or close to the main anthropogenic CO sources over the NH. In the observing domain for this constellation, we also detect some fire events, but during summer, several fires occur outside the constellation field of view that would require other (e.g., LEO) satellites to monitor and hence cannot be constrained using only GEO data assimilation.

3.2 Data assimilation impact

To assess the impact of assimilating the GEO constellation on global northern hemisphere CO, we first compare the full constellation assimilation run AR0 and the CR with the NR. Figures 5 and 6 show monthly averaged differences over the troposphere (surface to 200 hPa) of CR and AR0 with NR for winter and summer, respectively. In the same manner, figure 7 shows the same differences over the lower troposphere (surface to 800 hPa) just for February and July. Those plots show the overall biases of CR and AR0 versus NR, respectively. The CR runs show larger and more extended biases during winter than summer in the entire troposphere as well as in the lower troposphere. Despite stronger differences in emissions during summer between CR and NR (see figure 2), the shorter CO lifetime during summer reduces the global tropospheric bias. We can also observe this effect within the given seasons in figure 5 and 6. The CO lifetime shortens through January to March (and June to August) giving a reduced CR bias. With a shorter CO lifetime, errors owing to CO emissions have less persistence over time and propagation throughout the troposphere is less likely.

The AR0 reduces the overall CO bias in the NH troposphere. Figure 7 shows that a significant error reduction occurs at the lowest level of the atmosphere close to the sources over the GEO constellation fields of regard (see part I, figure 4 and figure 3 of this paper). As a result, data assimilation does not improve major error patterns close to the surface and out of the fields of regard (e.g., CO fire emissions close to Lake Baikal). A persistent error in the AR0 is still seen with patterns close to major cities or groups of cities over the 3 regions of interest. This shows that the DA system used here constrains CO fields close to CO sources, but that this system does not yet have the capability of updating the CO emission inventory. This means that while error reduction of the CO fields close to the surface is large, the errors are not removed since the un-adjusted model CO sources remain as an input to the error in the atmospheric CO fields. Assimilation of retrieved profiles close to the sources can provide a hemispheric constraint due to long-range transport of the relative increments and persistence over time of the error correction. In both seasons, global constraints take about a month for advection to spread the error correction over the NH. The level of improvement is also dependent on the CR bias. In the winter case study, the CR bias is larger than in the summer case study leading to the AR0 run being closer to the NR during summer compared to winter. Even if the error reduction is global, we observe large errors at the CO source locations because of remaining biases in emission inventories. For example, over Asia during July (summer), the cloud cover is high and hence the data density is too low to show significant improvement of the CO fields close to the surface. This effect is even more pronounced over the source regions that are not located in the observing domain of the GEO constellation, e.g. Siberian fires and Canadian fires.

Assimilation of a GEO-constellation of CO tropospheric measurement over the main NH anthropogenic sources allows a partial hemispheric constraint. Section 3.3 will quantify the performance of each satellite instrument.

3.3 Assimilation performance assessment

To quantify the effect of assimilation of the synthetic GEO-constellation observations, we define the skill score by the following metric:

$$SkillScore = 1 - \frac{\sum_t (AR - NR)^2}{\sum_t (CR - NR)^2}$$

This score is the ratio of the square error of the AR with respect to the CR over time *t*; we apply this to every grid cell of the CAM-Chem model. If the skill score is equal to 1, then the AR is perfect relative to the NR (AR equals NR). A positive value indicates that the square error of the AR is reduced by the ratio (or percentage) given by the skill score. If the skill score is zero, then the assimilation provides no changes; negative values indicate a degradation of the AR compared to the CR.

Figures 8 and 9 show the skill scores for the troposphere (surface to 200 hPa) for each month for winter and summer, respectively. We compute skill scores for the full constellation assimilation AR0, and for the single instrument observation experiments: AR1, AR2 and AR3. Data assimilation skill scores on single instrument assimilation (for AR1, AR2 and AR3) demonstrate the time required for a given instrument assimilation to impact the model tropospheric hemispheric CO. We identify two main patterns of transport affecting error reduction. The first pattern involves the Westerlies and warm conveyor belt processes at extratropical latitudes (AR1, AR2 and AR3). We clearly see this pattern over the first month of assimilation (January or June) crossing the Atlantic Ocean, the Asian continent and the Pacific Ocean from East to West. The second pattern involves the trade winds, which constrain tropical regions (AR1 and AR2 only) as they move from East to West over the tropical Pacific and the tropical Atlantic. Overall, the skill score shows improvement for every experiment, but to a different degree. In addition, we can see a degraded skill score away from the assimilated regions. This can be due to a bias sign change between the NR and the CR. If the overall assimilation effect is a positive bias (NR larger than CR) correction but a local negative bias is occurring (NR lower than CR) the assimilation run will show a degraded skill score in that particular case. Degraded skill scores are also due to coupled meteorology-chemistry processes represented in the CAM-Chem model. Adjusting the CO in a given region modifies the tropospheric chemistry budget, which can alter radiatively active species or provide a feedback on cloud formation and hence modify the meteorology. A modified meteorology can then affect the chemistry and hence change CO. This feedback is more obvious over lower latitudes and summer because of more complex dynamics at lower latitudes and chemistry that is more active during summer and at lower latitudes.

The winter fire event over South East Asia also illustrates these two effects. In this case, the fire plume is overestimated whereas a global underestimation (bias) of CO is provided by the CR. Assimilation of remote instruments from Asia will tend to increase the global CO, but will also contribute to an increase in CO in the fire plume and hence degrade the skill scores. In addition, high fire emissions generate a heavily polluted plume over the Pacific. Even slight changes in dynamics can generate large CO errors if the emission differences between the NR and CR are large, as it is the case between NR and CR emissions over Asia in March. In Figure 8 during March, the AR1 and AR2 (i.e., GEO-AS not assimilated) shows the signature of transported errors from the fire plumes, where a pattern of negative skill scores follows the large fire plume over the Pacific. In AR0 and AR3, where we assimilate the GEO-AS data, positive values above 0.6 replace the negative skill score pattern. This shows the importance of constraining the CO fields close to sources to generate improved remote CO fields, a result that is consistent with the conclusion of Barré et al. (2015b) using real data from MOPITT.

Figures 8 and 9 show large differences in the skill score magnitude over the NH. During winter, the CO lifetime is more than a factor of 2 longer than over summer (Shindell et al., 2006 and Edwards et al., 2004) due to oxidant loading which is greatest during the summer months. CO accumulates more during winter than during summer, leading to a more negative bias in the CR (see figures 5 and 6). The CR winter bias is larger than the CR summer bias even though emission differences are generally smaller during winter (Figure 2). Data assimilation relative increments, or the error reduction generated by assimilation close to the emission sources, then have more persistence over time during winter, and are advected throughout the entire troposphere. The AR0 skill scores show an average maximum around 0.7 during February 2006 (a month after starting the assimilation) and the pattern of improvement with respect to NR is relatively homogenous over the entire NH. During summer, July 2006 shows a 0.7 skill score over assimilated regions (GEO-US and GEO-EU), but the skill score is lower, down to 0.4, over remote regions. The reduction in long-range improvement in the AR0 during summer is also due to a lack of observational constraints over strong boreal fire sources that generate additional error variability in the CR relative to the NR. By looking at independent assimilation experiments (AR1, AR2, and AR3), the difference is even more noticeable.

As explained in section 2.2, cloud cover varies from one observed region to another, and depends on the season. GEO-US and GEO-EU show more data coverage during summer than during winter, and this tendency is opposite for GEO-AS. From the skill score seasonal tendency described above, cloud occurrence and hence data coverage is not the dominant factor determining skill scores. During winter, the CO lifetime is sufficiently long that less data density is sufficient to constrain the assimilation. Additionally, emission patterns and errors are mostly anthropogenic and have smaller variability and a more consistent geographical structure over time compared to fires. During summer, the CO lifetime is shorter and emission patterns are often more sporadic due to fires. However, during a given season, cloud cover affects the magnitude of the skill score. Over the GEO-AS footprint, the cloud free ratio is relatively low during summer (around 20% on average). This leads to lower skill scores for the summer AR3 experiment. In general, patterns of improvement are broader in space and larger during winter than summer, despite the reduced data sampling due to cloud cover over GEO-US and GEO-EU. During winter, the longer CO lifetime means that assimilating data from a single GEO instrument can provide a quasi-global improvement, which is not the case for summer.

4. Conclusions and perspectives

In this second part of our study we assessed the capability of a potential GEO constellation for monitoring atmospheric composition using an OSSE with a focus on measurements of CO. Part I of this study demonstrated that 3 GEO instruments measuring CO from space can be simulated realistically over three major anthropogenically active regions: CONUS, Western Europe and Eastern Asia. To perform the OSSE, we assimilated the synthetic constellation measurements into the CAM-Chem model-using DART. We first assessed differences between the CR and the NR, and found these to be reasonable based on global model biases, emissions and CO uncertainties according to literature on state-of-the-art global chemistry climate models. We designed assimilation experiments to assess the effects of long-range transport, seasonality, emissions and cloud cover on the capabilities of the GEO constellation to constrain CO concentrations. We designed two case studies of 3-month assimilation: winter (January-February-March) and summer (June-July-August). In addition to the control run (meteorological data assimilated only) and the full constellation assimilation experiment that we use as a benchmark, we also performed assimilation experiments for each instrument independently. In total, 10 data assimilation experiments led us to the following main conclusions:

1. Assimilation relative increments (posterior minus prior fields) are mostly located at or near the emission sources, and through long-range transport, these impact the entire NH troposphere. This result suggests that model errors in CO are largely due to emissions, which is consistent with previous data assimilation and modeling studies (Shindell et al., 2006; Fortems-Cheiney et al., 2011; Lamarque et al., 2012; Jiang et al., 2013; Barré et al., 2015b; Inness et al., 2015; Miyazaki et al., 2015; Tilmes et al., 2015). Each assimilated instrument shows improvement with respect to the CR in the CO transport patterns over large-scale areas associated with the westerly and trade winds at different latitudes.
2. The magnitude of the global impact depends on season. Winter data assimilation experiments show better improvement in CO NH distributions

than for summer. We explain this as follows. First, the CO lifetime during summer is shorter so that data assimilation relative increments have less persistence over time and less global advection within the model. Second, the summer has more large-scale fires in boreal regions, or away from the GEO constellation fields of regard. These fire emissions that are not captured by the GEO constellation are important to the global CO budget and variability.

3. Cloud cover affects the quality of the assimilated runs but this effect is not dominant when comparing summer and winter simulations. Winter shows a strong decrease of the cloud free ratio (number of cloud free scenes for a given pixel over a season) compared to summer for GEO-US and GEO-EU. This tendency is opposite for GEO-AS. However, the magnitude of the improvement with respect to the CR is still larger during winter due to CO lifetime, discussed in point 2 above. For summer, GEO-AS provides the lowest skill scores because of heavy cloud cover due to the Asian monsoon, and hence weak constraints from simulated CO observations.

This study assessed the observational requirements for CO, a good indicator of anthropogenic, fire and other natural emissions that have a lifetime long enough to allow transport between continents. Requirements are less demanding in terms of data density during winter compared to summer, and at wintertime extratropical latitudes compared to the tropics. Over the next decade, instruments will monitor atmospheric composition from geostationary platforms, (with temporal resolution on the order of minutes, but with coverage restricted to specific areas), and from LEO platforms that provide a global picture of the atmosphere but at lower temporal resolution (a revisit rate of 1 or 2 days). A next step of this study will be to assess the synergy between GEO and LEO platforms to constrain atmospheric CO composition and associated emissions from a global perspective. Assimilating the two different geometries in a single OSSE framework will provide a thorough scientific assessment.

Another focus for future work will be inferring emissions from GEO observations in order to provide accurate chemical forecasts near the surface. We will use the OSSE framework as presented here to assess the best method for emission source inversion using the ensemble Kalman filter (EnKF) technique. This will help define measurement requirements depending on emission types and their variability (e.g., anthropogenic emissions versus biomass burning). We will also investigate a combined CO and aerosol optical depth (AOD) assimilation with source inversion of carbonated aerosol species (black carbon and organic carbon).

Acknowledgements: This work was partly supported by NASA grants NNX09AH03G S02, NNX11AI10G *and* NNX11AG63G. The National Center for Atmospheric Reserch is sponsored by the National Science Foundation. The Climate Simulation Laboratory at NCAR's Computational and Information Systems Laboratory (CISL) provided computing resources. We would like to acknowledge high-performance computing support from Yellowstone (ark:/85065/d7wd3xhc) provided by NCAR's CISL. We also thank the reviewers for their constructive comments.

References

Anderson, J. L., Hoar, T., Raeder, K., Liu, H., Collins, N., Torn, R., and Arellano, A. (2009): The data assimilation testbed: a community facility, B. Am. Meteorol. Soc., 90, 1283–1296. doi: http://dx.doi.org/10.1175/2009BAMS2618.1

Barré, J., D. Edwards, H. Worden, A. Da Silva, W. Lahoz (2015a): On the feasibility of monitoring Carbon Monxide in the lower troposphere from a constellation of Northern Hemisphere geostationary satellites. (Part 1), doi:10.1016/j.atmosenv.2015.04.069

Barré, J., B. Gaubert, A. F. J. Arellano, H. M. Worden, D. P. Edwards, M. N. Deeter, J. L. Anderson, K. Raeder, N. Collins, S. Tilmes, et al. (2015b), Assessing the impacts of assimilating IASI and MOPITT CO retrievals using CESM-CAM-chem and DART, J. Geophys. Res. Atmos., 120, doi:10.1002/2015JD023467.

Bey, I., D. J. Jacob, R. M. Yantosca, J. A. Logan, B. D. Field, A. M. Fiore, Q. Li, H. Y. Liu, L. J. Mickley, and M. G. Schultz (2001), Global modeling of tropospheric chemistry with assimilated meteorology: Model description and evaluation, J. Geophys. Res., 106(D19), 23073–23095, doi:10.1029/2001JD000807.

Bian, H., M. Chin, S. R. Kawa, B. Duncan, A. Arellano, and P. Kasibhatla (2007), Sensitivity of global CO simulations to uncertainties in biomass burning sources, J. Geophys. Res., 112, D23308, doi:10.1029/2006JD008376.

Claeyman, M., Attié, J.-L., Peuch, V.-H., El Amraoui, L., Lahoz, W. A., Josse, B., Joly, M., Barré, J., Ricaud, P., Massart, S., Piacentini, A., von Clarmann, T., Höpfner, M., Orphal, J., Flaud, J.- M., and Edwards, D. P.: A thermal infrared instrument onboard a geostationary platform for CO and O3 measurements in the lowermost troposphere: Observing System Simulation Experiments (OSSE), Atmos. Meas. Tech., 4, 1637–1661, doi:10.5194/amt-4-1637-2011, 2011a.

Conley, A. J., et al. (2012), Description of the NCAR Community Atmosphere Model (CAM 5.0). NCAR technical note

Duncan, B. N., D. Portman, I. Bey, and C. M. Spivakovsky (2000), Parameterization of OH for efficient computation in chemical tracer models, J. Geophys. Res., 105, 12,259–12,262.

Edwards, D. P., et al. (2004), Observations of carbon monoxide and aerosol from the Terra satellite: Northern Hemisphere variability, J. Geophys. Res., 109, D24202, doi:10.1029/2004JD004727.

Edwards, D. P., Arellano Jr., A. F., and Deeter, M. N.: A satellite observation system simulation experiment for carbon monoxide in the lowermost troposphere, J. Geophys. Res., 114, D14304, doi:10.1029/2008JD011375, 2009.

Emmons, L. K., Walters, S., Hess, P. G., Lamarque, J.-F., Pfister, G. G., Fillmore, D., Granier, C., Guenther, A., Kinnison, D., Laepple, T., Orlando, J., Tie, X., Tyndall, G., Wiedinmyer, C., Baughcum, S. L., and Kloster, S. (2010): Description and evaluation of the Model for Ozone and Related chemical Tracers, version 4 (MOZART-4), Geosci. Model Dev., 3, 43-67, doi:10.5194/gmd-3-43-2010, 2010.

Fortems-Cheiney, A., F. Chevallier, I. Pison, P. Bousquet, S. Szopa, M. N. Deeter, and C. Clerbaux (2011), Ten years of CO emissions as seen from Measurements of Pollution in the Troposphere (MOPITT), J. Geophys. Res., 116, D05304, doi:10.1029/2010JD014416.

Guenther, A. B., Jiang, X., Heald, C. L., Sakulyanontvittaya, T., Duhl, T., Emmons, L. K., and Wang, X. (2012): The Model of Emissions of Gases and Aerosols from Nature version 2.1 (MEGAN2.1): an extended and updated framework for modeling biogenic emissions, Geosci. Model Dev., 5, 1471-1492, doi:10.5194/gmd-5-1471-2012.

Inness, A., Blechschmidt, A.-M., Bouarar, I., Chabrillat, S., Crepulja, M., Engelen, R. J., Eskes, H., Flemming, J., Gaudel, A., Hendrick, F., Huijnen, V., Jones, L., Kapsomenakis, J., Katragkou, E., Keppens, A., Langerock, B., de Mazière, M., Melas, D., Parrington, M., Peuch, V. H., Razinger, M., Richter, A., Schultz, M. G., Suttie, M., Thouret, V., Vrekoussis, M., Wagner, A., and Zerefos, C.: Data assimilation of satellite-retrieved ozone, carbon monoxide and nitrogen dioxide with ECMWF's Composition-IFS, Atmos. Chem. Phys., 15, 5275-5303, doi:10.5194/acp-15-5275-2015, 2015.

Jiang, Z., Jones, D., Worden, H., Deeter, M., Henze, D., Worden, J., Bowman, K., Brenninkmeijer, C. and Schuck, T.: Impact of model errors in convective transport on CO source estimates inferred from MOPITT CO retrievals, J. Geophys. Res. Atmos., 118(4), 2073–2083, doi:10.1002/jgrd.50216, 2013.

Lamarque, J.-F., Bond, T. C., Eyring, V., Granier, C., Heil, A., Klimont, Z., Lee, D., Liousse, C., Mieville, A., Owen, B., Schultz, M. G., Shindell, D., Smith, S. J., Stehfest, E., Van Aardenne, J., Cooper, O. R., Kainuma, M., Mahowald, N., McConnell, J. R., Naik, V., Riahi, K., and van Vuuren, D. P. (2010): Historical (1850–2000) gridded anthropogenic and biomass burning emissions of reactive gases and aerosols: methodology and application, Atmos. Chem. Phys., 10, 7017-7039, doi:10.5194/acp-10-7017-2010.

Lamarque, J.-F., Emmons, L. K., Hess, P. G., Kinnison, D. E., Tilmes, S., Vitt, F., Heald, C. L., Holland, E. A., Lauritzen, P. H., Neu, J., Orlando, J. J., Rasch, P. J., and Tyndall, G. K. (2012): CAM-chem: description and evaluation of interactive atmospheric chemistry in the Community Earth System Model, Geosci. Model Dev., 5, 369-411, doi:10.5194/gmd-5-369-2012.

Miyazaki, K., Eskes, H. J., and Sudo, K.: A tropospheric chemistry reanalysis for the years 2005–2012 based on an assimilation of OMI, MLS, TES, and MOPITT satellite data, Atmos. Chem. Phys., 15, 8315-8348, doi:10.5194/acp-15-8315-2015, 2015.

Ott, L., B. Duncan, S. Pawson, P. Colarco, M. Chin, C. Randles, T. Diehl, and E. Nielsen, 2010: Influence of the 2006 Indonesian biomass burning aerosols on tropical dynamics studied with the GEOS-5 AGCM. J. Geophys. Res., 115, D14121, doi:10.1029/2009JD013181.

Putman, W., A. M. da Silva, L. E. Ott, and A. Darmenov, 2014: Model Configuration for the 7-km GEOS-5.12 Nature Run, Ganymed Release (Non-hydrostatic 7 km Global Mesoscale Simulation), GMAO Office Note, bf 5. (Version 1.0), 86 pp, available from http://gmao.gsfc.nasa.gov/pubs/office notes.

Raeder, Kevin, Jeffrey L. Anderson, Nancy Collins, Timothy J. Hoar, Jennifer E. Kay, Peter H. Lauritzen, and Robert Pincus, (2012): DART/CAM: An Ensemble Data Assimilation System for CESM Atmospheric Models. J. Climate, 25, 6304–6317. doi: http://dx.doi.org/10.1175/JCLI-D-11-00395.1

Shindell, D. T., et al. (2006): Multimodel simulations of carbon monoxide: Comparison with observations and projected near-future changes , J. Geophys. Res., 111, D19306, doi:10.1029/2006JD007100.

Stein, O., Schultz, M. G., Bouarar, I., Clark, H., Huijnen, V., Gaudel, A., George, M., and Clerbaux, C. (2014): On the wintertime low bias of Northern Hemisphere carbon monoxide found in global model simulations, Atmos. Chem. Phys., 14, 9295-9316, doi:10.5194/acp-14-9295-2014.

Strode, S. A., Duncan, B. N., Yegorova, E. A., Kouatchou, J., Ziemke, J. R., and Douglass, A. R. (2015): Implications of carbon monoxide bias for methane lifetime and atmospheric composition in chemistry climate models, Atmos. Chem. Phys., 15, 11789-11805, doi:10.5194/acp-15-11789-2015.

Tilmes, S., Lamarque, J.-F., Emmons, L. K., Kinnison, D. E., Ma, P.-L., Liu, X., Ghan, S., Bardeen, C., Arnold, S., Deeter, M., Vitt, F., Ryerson, T., Elkins, J. W., Moore, F., Spackman, J. R., and Val Martin, M. (2015): Description and evaluation of tropospheric chemistry and aerosols in the Community Earth System Model (CESM1.2), Geosci. Model Dev., 8, 1395-1426, doi:10.5194/gmd-8-1395-2015, 2015.

Timmermans, R.M.A., W.A. Lahoz, J.-L. Attié, V.-H. Peuch, R.L. Curier, D.P. Edwards, H.J. Eskes, P.J.H. Builtjes, Observing System Simulation Experiments for air quality, Atmospheric Environment 05/2015; 115. DOI:10.1016/j.atmosenv.2015.05.032

Wiedinmyer, C., Akagi, S. K., Yokelson, R. J., Emmons, L. K., Al-Saadi, J. A., Orlando, J. J., and Soja, A. J. (2001): The Fire INventory from NCAR (FINN): a high resolution global model to estimate the emissions from open burning, Geosci. Model Dev., 4, 625-641, doi:10.5194/gmd-4-625-2011.

Zoogman, P., Jacob, D. J., Chance, K., Zhang, L., Le Sager, P., Fiore, A. M., Eldering, A., Liu, X., Natraj, V., and Kulawik, S. S.: Ozone Air Quality Measurement Requirements for a Geostationary Satellite Mission, Atmos. Environ., 45, 7143–7150, doi:10.1016/j.atmosenv.2011.05.058, 2011.

Zoogman, P., D.J. Jacob, K. Chance, H.M. Worden, D.P. Edwards, L. Zhang, Improved monitoring of surface ozone air quality by joint assimilation of geostationary satellite observations of ozone and CO. Atmospheric Environment, 84, 254-261, 2014.

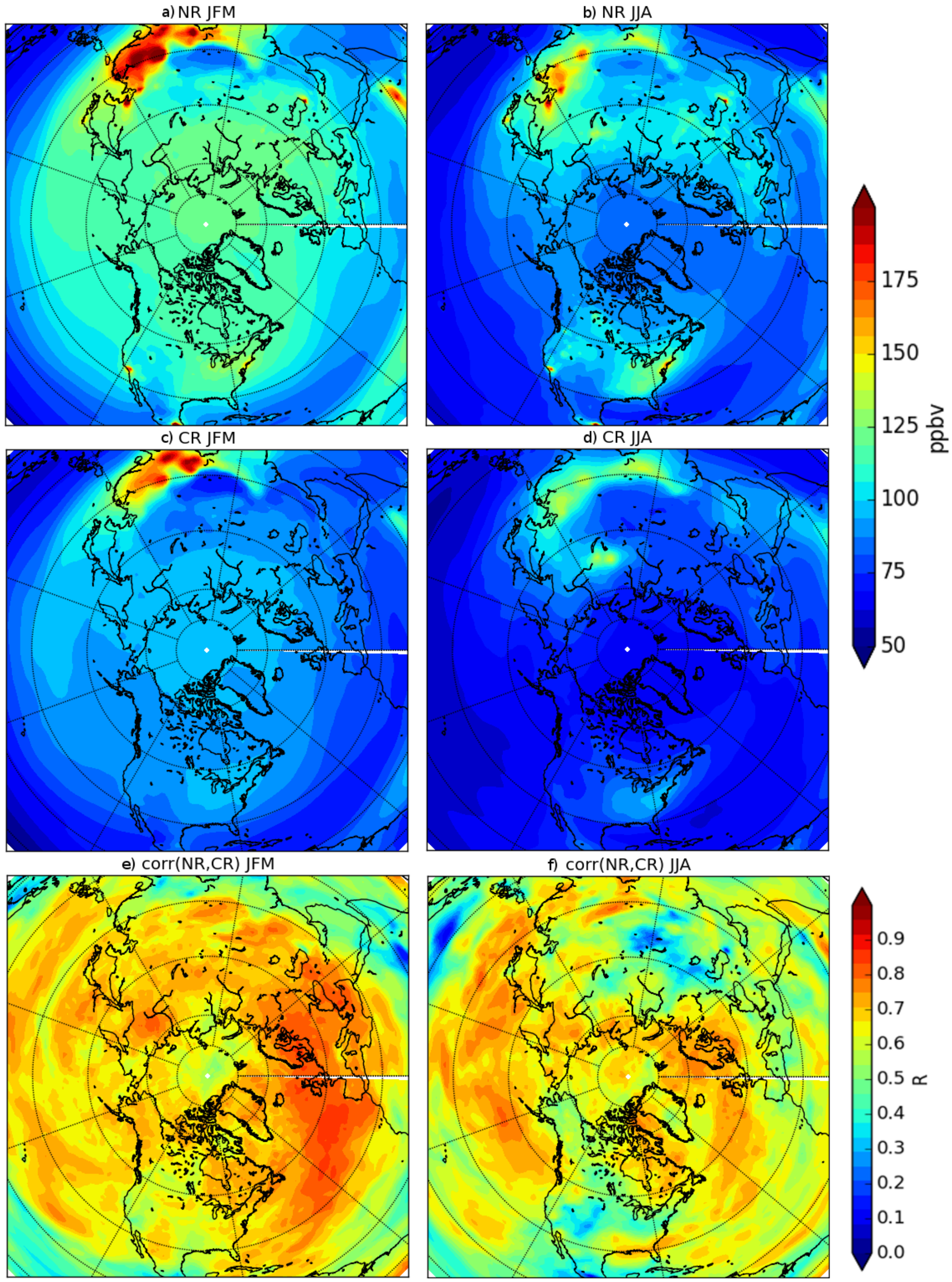

Figure 1. Plots of the Nature Run (NR) and the Control Run (CR) January-February-March (JFM) a) and c), respectively, and June-July-August (JJA) b) and d), respectively. We convert mean values of Surface-200hPa tropospheric CO column into a pseudo volume mixing ratio. Red and blue colors refer to relatively high and low values, respectively. Bottom panels show the correlation coefficient R between the NR and CR for JFM (e) and JJA (f), respectively.

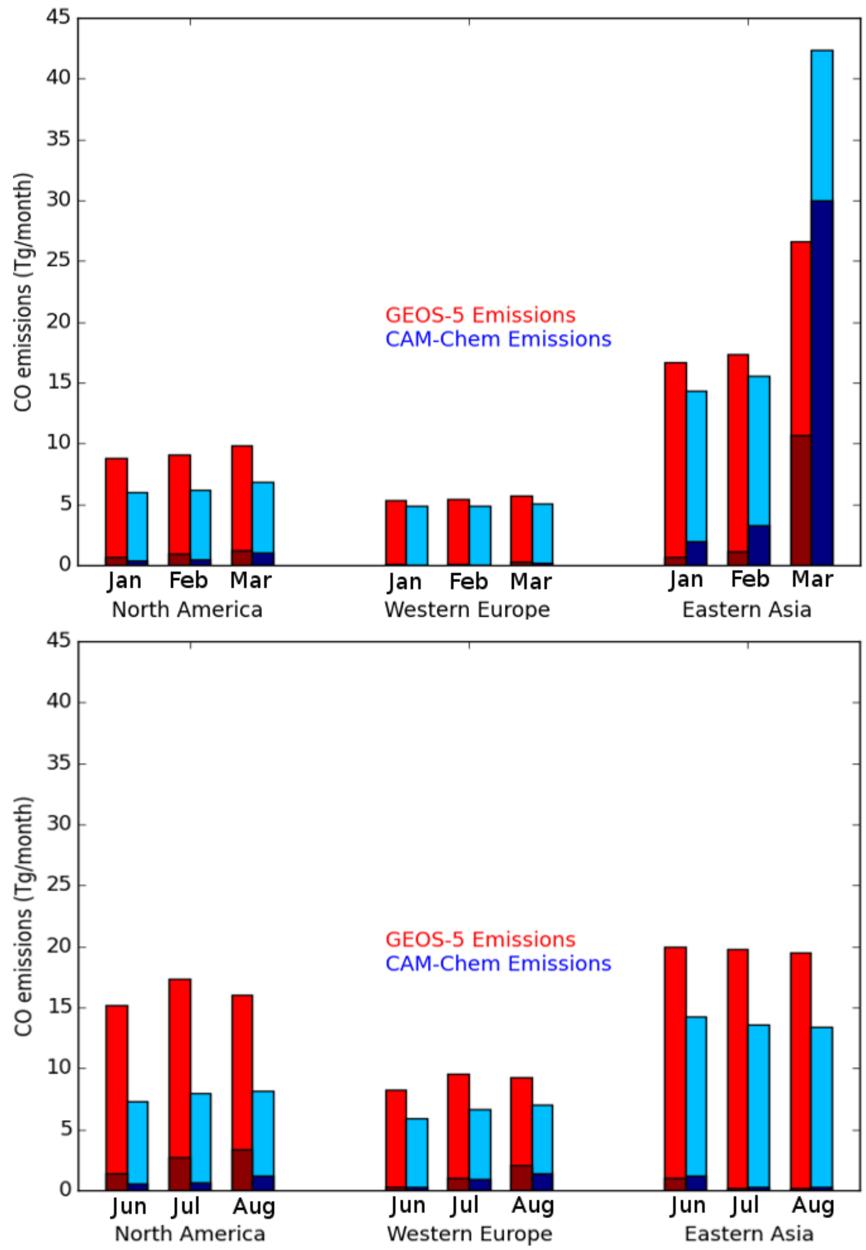

Figure 2. Monthly emission estimated budgets derived from emission inventories for winter (top panel) and summer (bottom panel) 2006 for GEOS-5 (red) and CAM-Chem (blue) in Teragrams (Tg) of CO per month. Dark colors indicate the biomass-burning fraction of the emission budgets.

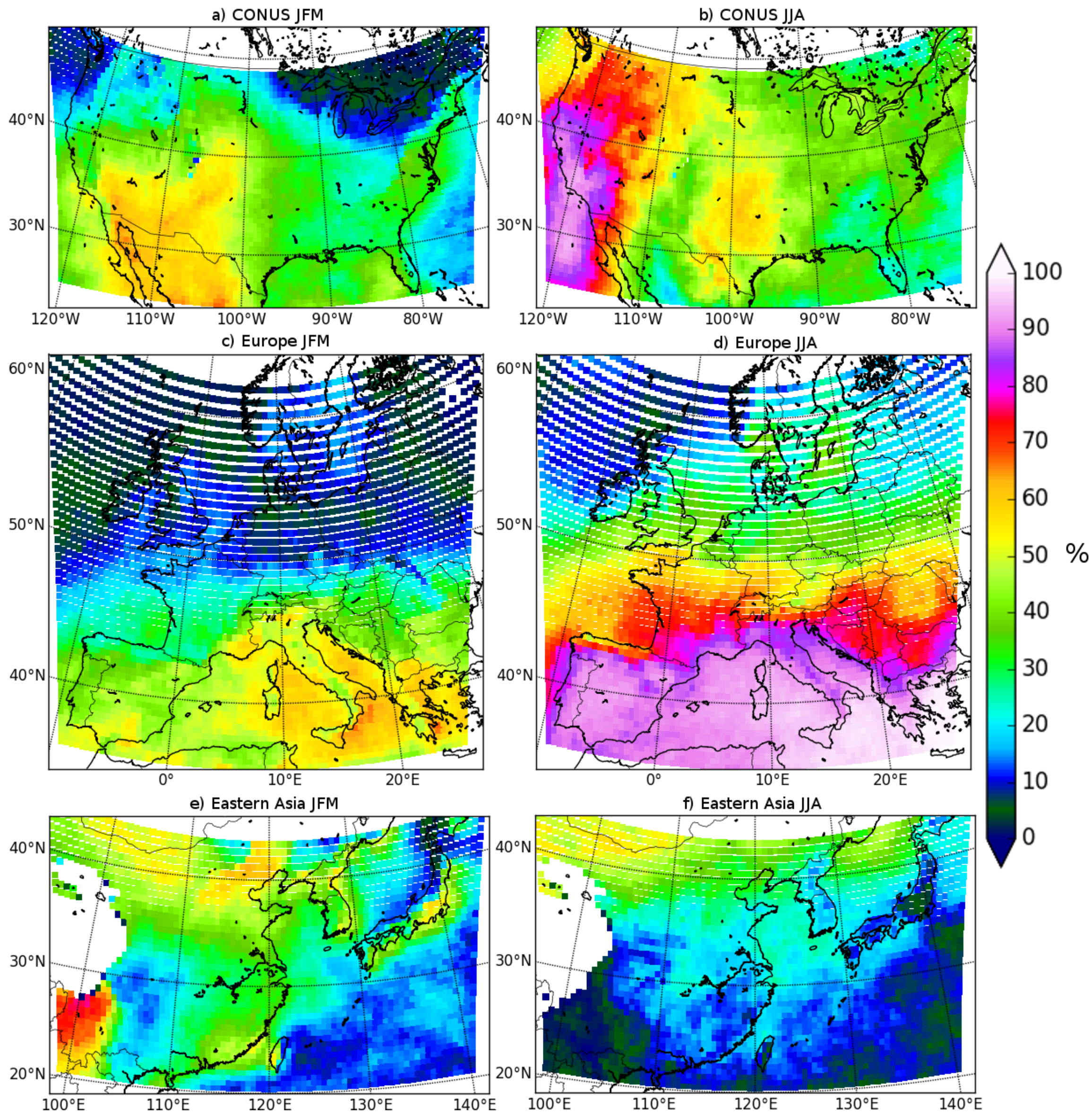

Figure 3. Cloud free ratio in % for the three geostationary instruments for the winter (left) and summer (right) seasons. Top panels (a and b) refer to the CONUS; middle panels (c and d) refer to Europe; bottom panels (e and f) refer to Eastern Asia. Red/purple and blue colors refer to relatively high and low values, respectively.

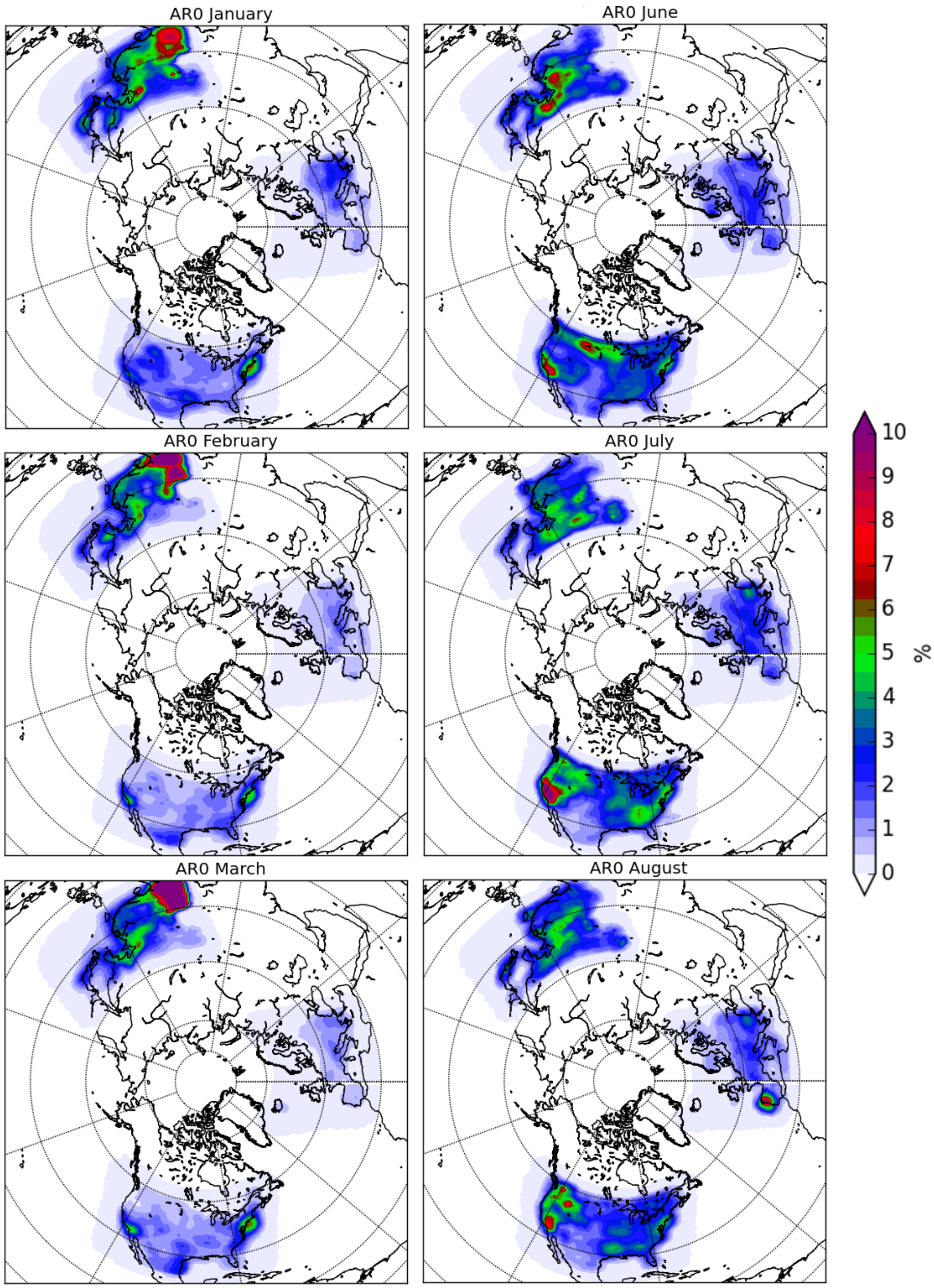

Figure 4. RMS of relative increments in % (posterior state minus prior state divided by the prior state) between the surface to 200 hPa during January, February and March 2006 (top to bottom, left) and during June, July, August 2006 (top to bottom, right). Red and blue colors refer to relatively high and low values, respectively.

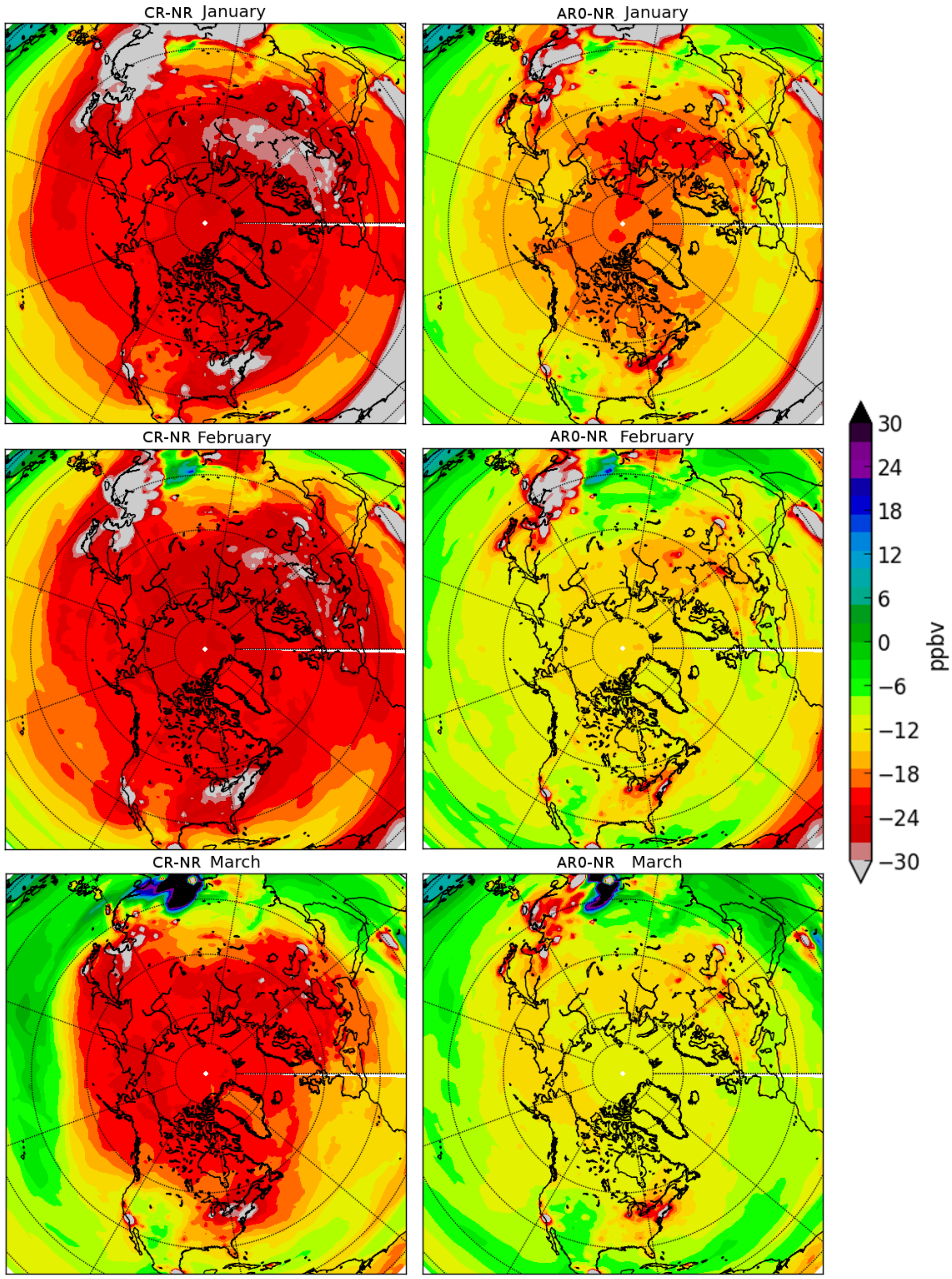

Figure 5. Average differences in the tropospheric (surface to 200 hPa) CO fields between the control run (CR) and the nature run (NR) on the left hand side and average differences between full constellation assimilated CO (AR0) and the nature run (NR) on the right hand side during January, February and March (top to bottom) 2006. Units are ppbv.

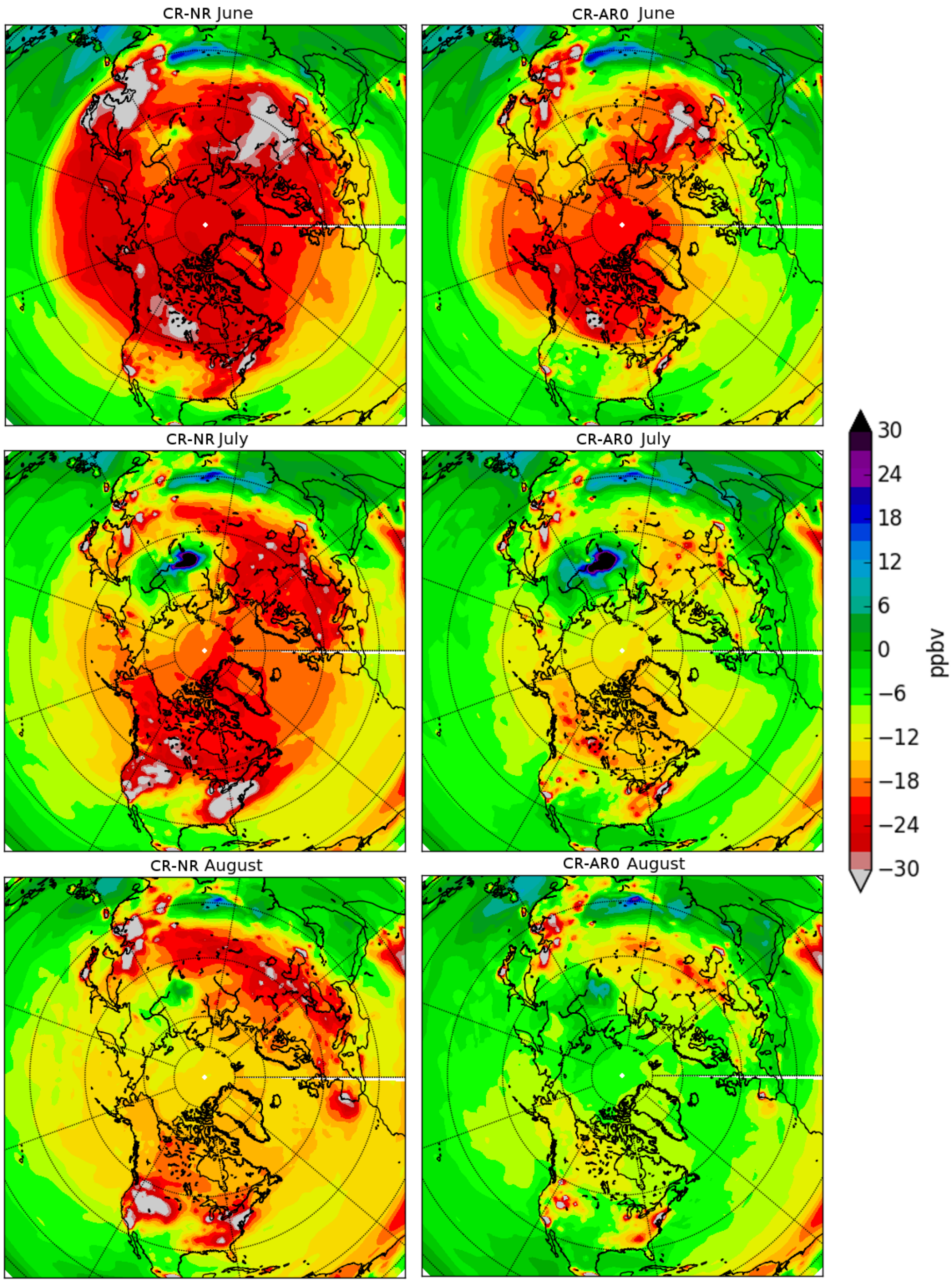

Figure 6. Same as Fig. 5 but for June, July and August 2006.

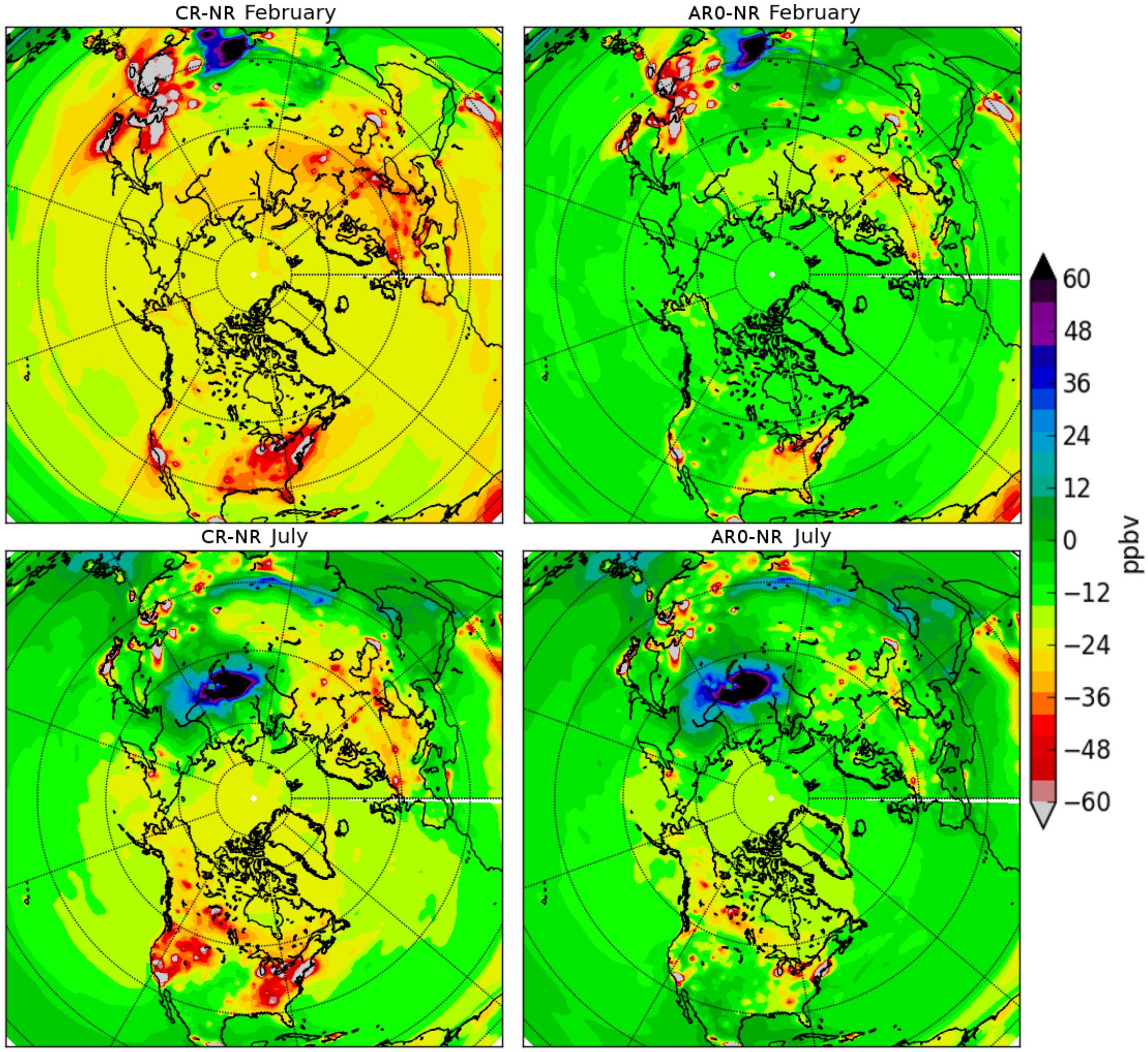

Figure 7. Average differences in the lower tropospheric (surface to 800 hPa) CO fields between the control run (CR) and the nature run (NR) on the left hand side and average differences between full constellation assimilated CO (AR0) and the nature run (NR) on the right hand side during February and July (top and bottom, respectively) 2006. Units are ppbv.

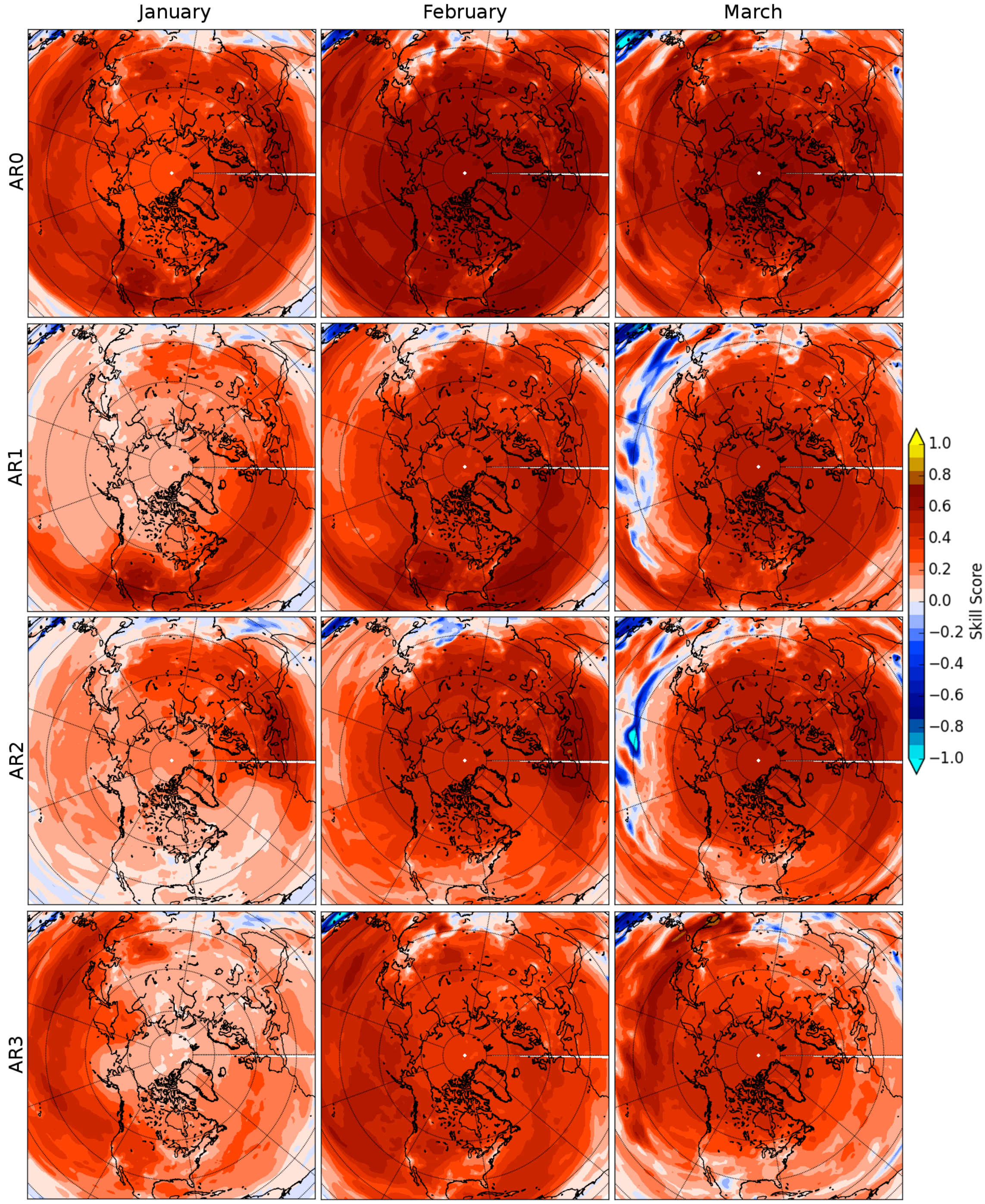

Figure 8. Assimilation skill scores (see text for details) for the full constellation assimilation (AR0, first row), GEO-US assimilated only (AR1, second row), GEO-EU assimilated only (AR2, third row) and GEO-AS assimilated only (AR3, fourth row). Surface to 200hPa and monthly statistics are performed during winter: January (first column), February (second column) and March (third column) 2006. Red and blue colors refer to positive and negative skill scores, respectively.

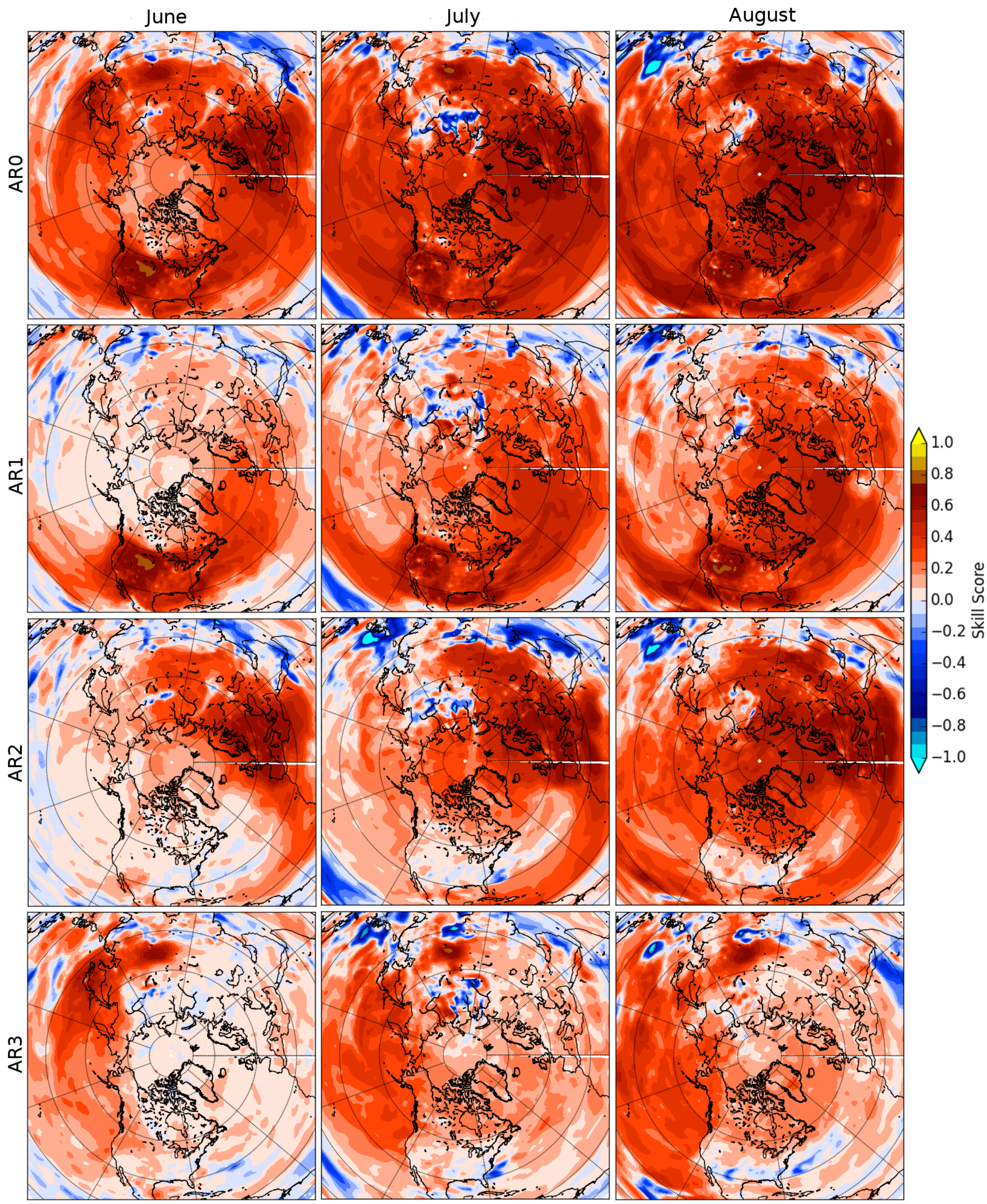

Figure 9. Same as Figure 8. but for summer: June (first columns), July (second column) and August (third column) 2006.